Title

Restricted and unrestricted non-Hermitian Hartree-Fock: Theory, practical considerations, and applications to metastable molecular anions.

Journal

The Journal of chemical physics, 143(7)

ISSN

0021-9606

Authors

White, Alec F
McCurdy, C William
Head-Gordon, Martin

Publication Date

2015-08-01

DOI

10.1063/1.4928529

Peer reviewed

Restricted and unrestricted non-Hermitian Hartree-Fock: theory, practical considerations, and applications to metastable molecular anions

Alec F. White,[1] C. William McCurdy,[2,3] and Martin Head-Gordon[4]

[1)] *Kenneth S. Pitzer Center for Theoretical Chemistry, Department of Chemistry, University of California, Berkeley and Chemical Sciences Division, Lawrence Berkeley National Laboratory, Berkeley, California 94720, USA*

[2)] *Chemical Sciences Division and Ultrafast X-ray Science Laboratory, Lawrence Berkeley National Laboratory, Berkeley CA 94720*

[3)] *Department of Chemistry, University of California, Davis, CA 95616 USA*

[4)] *Department of Chemistry, University of California, Berkeley and Chemical Sciences Division, Lawrence Berkeley National Laboratory, Berkeley, California 94720, USA*

(Dated: 15 July 2015)

This work describes the implementation and applications of non-Hermitian self-consistent field (NH-SCF) theory with complex basis functions for the *ab initio* computation of positions and widths of shape resonances in molecules. We utilize both the restricted open-shell and the previously unexplored spin-unrestricted variants to compute Siegert energies of several anionic shape resonances in small diatomic and polyatomic molecules including carbon tetrafluoride which has been the subject of several recent experimental studies. The computation of general molecular properties from a non-Hermitian wavefunction is discussed, and a density-based analysis is applied to the $^2B_1$ shape resonance in formaldehyde. Spin-unrestricted NH-SCF is used compute a complex potential energy surface for the carbon monoxide anion which correctly describes dissociation.

PACS numbers: 34.80.Bm, 34.20.-b, 32.80.Zb 33.80.Eh

I. INTRODUCTION

Metastable electronic states, or resonances, in molecules play an important role in a variety of chemical processes. They can be described by a Siegert energy:

$$E = \mathcal{E} - i\frac{\Gamma}{2} \tag{1}$$

where $\mathcal{E}$ is the position and Γ is the width of the resonance. Unfortunately, due to their continuum nature, these states have largely eluded large-scale, reliable computation. Many of the most promising candidates for reliable computation of Siegert energies are based on complex-coordinate methods.[1–3]

Originally based on the mathematically rigorous theorems of Aguilar, Balsev, and Combes,[4,5] and Simon,[6] these methods rely on the solution of a non-Hermitian effective Hamiltonian. This effective Hamiltonian is constructed so as to contain in its spectrum complex eigenvalues equal to the Siegert energies and corresponding to square integrable eigenfunctions. This process, which generally involves the scaling of some of the coordinates of the Hamiltonian by a complex number, is called complex-scaling. Unfortunately, non-analyticities arising from the Born-Oppenheimer approximation make the application to molecular systems difficult.[7–9] This problem can be overcome with the mathematically rigorous method of exterior complex scaling.[8]

Though difficult to apply direcctly, the exterior complex-scaling transformation can be implicitly applied using complex basis functions.[7,10] In this method, complex Gaussian functions of the form

$$\begin{aligned}\phi_\theta(r) = N(\theta)(x - A_x)^l(y - A_y)^m(z - A_z)^n \\ \times \exp\left[-\alpha e^{-2i\theta}(\mathbf{r} - \mathbf{A})^2\right]\end{aligned} \tag{2}$$

are included in the basis set. The method of complex basis functions has been applied to a variety of diatomic molecules[7,11–18] and has recently been applied to some larger, polyatomic molecules in the static exchange (SE) approximation.[10] In this study, we employ complex basis functions in computations on electronic shape resonances in molecules.

Complex coordinate methods, as they are usually used, reduce the full scattering problem to a variational search within a basis of square integrable functions. Unfortunately, in many electron systems one is almost always forced to make further approximations to make the

many-body problem computationally feasible. In quantum chemistry, it is the self-consistent field (SCF) wavefuction that usually serves as a first approximation and as a starting point for more accurate methods. The SCF method was first introduced in the context of complex coordinate methods by McCurdy *et al.*[19] For metastable anions, these methods explicitly treat the polarization of the target molecule or atom due to the presence of an additional electron at a mean-field level. While these methods are usually called complex SCF or complex-scaled SCF, we will refer to them as non-Hermitian SCF (NH-SCF) methods so as to highlight the non-Hermitian nature of the problem and to avoid confusion with complex Hermitian SCF methods.

NH-SCF methods have been successfully applied in the context of straight complex-scaling to a variety of atomic shape resonances.[19–24] NH-SCF methods employing complex basis functions have also been applied to shape resonances in a variety of diatomic molecules.[11–13,16] Various types of non-Hermitian DFT methods have also been recently developed.[25–28] While SCF-type methods are not directly applicable to Feshbach resonances, non-Hermitian multiconfigurational self-consistent field (NH-MCSCF)[29,30] or non-Hermitian configuration interaction (NH-CI)[31–33] approaches have been successfully applied to Feshbach resonances in atoms. For molecules, these multi-determinental methods have also been shown to provide a description of Feshbach resonances.[14–18] Recently, complex scaled coupled-cluster methods have also been been used for shape and Feshbach resonances in atoms.[34,35]

In this study, we discuss in detail the implementation and application of NH-SCF theory to molecular anionic shape resonances. After reviewing the non-Hermitian version of restricted open-shell Hartree-Fock (NH-ROHF), we introduce the spin-unrestricted variant (NH-UHF) and apply both to a variety of small diatomic and polyatomic molecules. This is the first time that this method has been applied to polyatomic molecules. Additionally, we include a discussion of the calculation and interpretation of general molecular properties from a non-Hermitian wavefunction. A density based analysis and visualization of the electron attachment process is introduced and applied to the $^2B_1$ resonance in formaldehyde. Finally, we use NH-UHF to compute a complex potential energy surface for the carbon monoxide anion. Like its Hermitian counterpart, NH-UHF theory is found to be capable of describing full potential energy surfaces with qualitative accuracy.

II. THEORY

The theoretical background of NH-SCF is described in detail in other works.[19,20] Here we augment these discussions with a derivation in terms of the complex variational principle[36–38] which, in the context of complex basis functions, states that the Siegert energy of some trial, c-normalizable function $|\Psi)$,

$$E = \frac{(\Psi|H|\Psi)}{(\Psi|\Psi)}, \tag{3}$$

is stationary with respect to small variations about the true wavefunction. In the method of complex basis functions, the "true" wavefunction is the true exterior scaled wavefuction evaluated in a transformed variable as discussed in Ref. 10. The brackets $(\ldots|\ldots)$ are used to denote the c-product,[37] which means that the bra is not complex-conjugated. A complex NH-SCF energy is determined by requiring that the energy functional of equation 3 is made stationary to first order with respect to variations of a single Slater determinant trial wavefunction. This Slater determinant is constructed from molecular orbitals (MOs) that are constrained to be c-orthonormal. This gives rise to a Lagrangian

$$\mathcal{L} = (\Psi|H|\Psi) - \sum_{ij} \left[(\phi_i|\phi_j) - \delta_{ij}\right] \lambda_{ij} \tag{4}$$

where the many body state $|\Psi)$ is chosen to be a single Slater determinant of MOs $\phi_i(\mathbf{r})$, and the λ_{ij} are Lagrange multipliers. The MOs are c-orthonomal functions constructed from real and complex Gaussian basis functions as described in Ref 10. As in the real case, the specification of any constraints on the spin part of the wavefunctions, followed by the extremization of $\mathcal{L}$, gives rise to the NH-SCF equations.

A. NH-ROHF and NH-UHF equations

The NH-ROHF equations are the same as in the real case.[39] Stationarity of the Lagrangian of Equation 4 gives rise to the NH-ROHF equations presented in Ref. 19. For the Hermitian analog, see Ref. 40. These equations are represented by a single Fock matrix of the form

$$\mathbf{F} = \begin{pmatrix} \mathbf{R}_{cc} & \mathbf{F}_{co} & \mathbf{F}_{cv} \\ \mathbf{F}_{oc} & \mathbf{R}_{oo} & \mathbf{F}_{ov} \\ \mathbf{F}_{vc} & \mathbf{F}_{vo} & \mathbf{R}_{vv} \end{pmatrix} \tag{5}$$

where the off-diagonal parts are

$$\begin{aligned} \mathbf{F}_{co} &= \mathbf{F}^{\beta} \\ \mathbf{F}_{cv} &= \mathbf{F}^{\alpha} + \mathbf{F}^{\beta} \\ \mathbf{F}_{ov} &= \mathbf{F}^{\alpha} \end{aligned} \tag{6}$$

in terms of the α and β Fock matrices from UHF theory. There is some ambiguity in the specification of the diagonal blocks of the Fock matrix (see Refs. 39 and 41) which can be exploited to improve convergence.[40] The diagonal terms are chosen to be:

$$\begin{aligned} \mathbf{R}_{cc} &= \mathbf{F}^{\alpha} + \mathbf{F}^{\beta} \\ \mathbf{R}_{oo} &= \mathbf{F}^{\beta} \\ \mathbf{R}_{vv} &= \mathbf{F}^{\alpha} + \mathbf{F}^{\beta}. \end{aligned} \tag{7}$$

This somewhat unconventional choice was found to have good convergence properties.

The NH-UHF equations are the same as in standard Hermitian UHF theory.[42] The α and β Fock matrices are given by

$$\begin{aligned} \mathbf{F}^{\alpha} &= \mathbf{h} + \mathbf{J}^{\alpha} + \mathbf{J}^{\beta} - \mathbf{K}^{\alpha} \\ \mathbf{F}^{\beta} &= \mathbf{h} + \mathbf{J}^{\alpha} + \mathbf{J}^{\beta} - \mathbf{K}^{\beta} \end{aligned} \tag{8}$$

where $\mathbf{J}^{\alpha}$ and $\mathbf{K}^{\alpha}$ are the Coulomb and exchange matrices generated from just the α electron density and those operators constructed from the β density are similarly defined. $\mathbf{h}$ is the basis set representation of the core Hamiltonian. These operators are distinguished from their Hermitian counterparts in that the matrix elements are computed with the c-norm.

The c-norm, while convenient, is somewhat restrictive in that it represents an analytic continuation of matrix elements of a real, symmetric Hamiltonian.[37] However, it has long been known that complex MO coefficients are sometimes necessary to describe certain forms of symmetry breaking within the purely Hermitian formalism of traditional electronic structure theory.[43,44] In these cases, the Fock matrix becomes complex Hermitian. In order to include in our description the degrees of freedom relevant to complex-Hermitian Hartree-Fock calculations, a more general bi-orthogonal space must be considered. While this would certainly be an interesting extension, it is not relevant to the examples presented in this study.

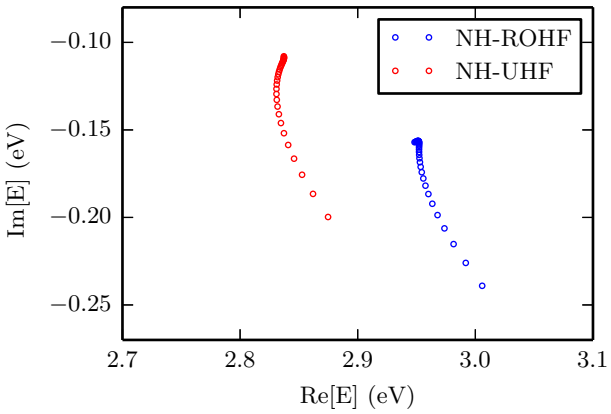

FIG. 1. Representative θ-trajectories for N_2^- in the caug-cc-pVDZ(cm+) basis set. The complex basis function parameter, θ, is varied from $10^o \ldots 25^o$ in increments of 0.5^o. The approximate location of the stationary point is $(2.8, -0.1)$ for NH-UHF, while for NH-ROHF, it is $(2.9, -0.15)$.

B. Practical considerations in the optimization of NH-SCF wavefunctions

The NH-SCF equations, like their Hermitian counterparts, will have continuum solutions. Special care must therefore be taken with the initial guess and the method of iteration so as to ensure convergence to the desired resonance state. It is important to emphasize that the desired solutions are not minima of Equation 3.

The natural starting point for an NH-SCF calculation is an SE result. Here, the procedure described in Ref. 10 was used to generate a guess density for the metastable anion. This is the same method employed in previous studies.[11,19] In order to converge preferentially to a Siegert energy that is stationary but not in any way a minimum, an overlap criterion similar to that of Gilbert *et al.*[45] was used to select the appropriate occupied space after each iteration.

In previous applications of NH-SCF, little is reported regarding convergence properties and simple iteration was generally found to yield convergent results. These studies differ from this work in that the basis sets were generally smaller and the complex functions were added only in a particular symmetry. We found that simple iteration only converged to the desired state in very few cases even when small basis sets were used. The direct inversion of the iterative subspace (DIIS) method of Pulay[46,47] was found to be significantly more reliable.

The DIIS method, as it is usually applied to SCF convergence, computes an extrapo-

lated Fock matrix as a linear combination of Fock matrices from previous iterations. The relative weights are determined by requiring that they minimize an error vector, which is also computed at each iteration, subject to a normalization constraint. In the standard SCF problem, this error vector (in this case a matrix) is usually taken to be

$$\mathbf{e} = \mathbf{SPF} - \mathbf{FPS} \tag{9}$$

where $\mathbf{S}$, $\mathbf{P}$ and $\mathbf{F}$ indicate the overlap, density, and Fock matrices respectively. The elements of this vector are elements of the orbital rotation gradient in the AO basis. In the non-Hermitian case, this method can be used with little modification because the (complex) orbital rotation gradient must still be zero at convergence which suggests that the error vector of equation 9 is still appropriate. In the non-Hermitian case the error vector is split into real and imaginary parts, and the real and imaginary parts of the extrapolated Fock matrix are found in the iterative subspace. In practice, an orthogonalized error vector is used to give a more balanced description of the error.

Unfortunately, the solution of the NH-SCF equations at a single value of θ will in general not yield a good approximation to the Siegert energy. In practice, the NH-SCF energy is computed at many values of θ and an analytic continuation scheme[10,48] is used to compute the energy at the optimal value of θ. An example of these θ-trajectories is shown in Figure 1.

C. Properties of NH-SCF states

In the method of complex basis functions and in other complex-coordinate techniques, the wavefunction is not the true wavefunction of the system and is in fact not a physically realizable state of any kind. In this section, we briefly describe how properties of the resonance can be extracted from the non-Hermitian wavefunction in terms of the response of the complex Siegert energy.

Moiseyev *et al.*[37] showed that there exists an analog to the Hellmann-Feynman theorem in a c-normalizable space. It implies, in the context of complex basis functions, that given some Hamiltonian perturbed by some operator V with strength α,

$$H(\alpha) = H_0 + \alpha V, \tag{10}$$

the derivative of the energy with respect to α is

$$\frac{dE}{d\alpha} = (\Psi|V|\Psi) \tag{11}$$

given that $|\Psi)$ is variationally optimized and normalized, and that the complex basis functions are independent of V (i.e. no Pulay terms[49]). The c-expectation value will in general have both real and imaginary parts, but those parts are easily associated with the response of the position and width respectively:

$$\frac{d\mathcal{E}}{d\alpha} = \mathrm{Re}(\Psi|V|\Psi) \qquad \frac{d\Gamma}{d\alpha} = -2\mathrm{Im}(\Psi|V|\Psi). \tag{12}$$

Note that both these quantities are, at least in theory, observable.

For one-electron properties, the c-expectation value can be written as

$$(\Psi|V|\Psi) = \sum_{\mu\nu} V_{\mu\nu} P^{\nu\mu} \tag{13}$$

where μ and ν index AO basis functions and $\mathbf{V}$ and $\mathbf{P}$ are the AO matrix representations of operator V and the 1-particle density respectively. The c-normalization of the wave function implies that the 1-particle density matrix defined with the same complex inner product has a real part with a trace equal to the number of electrons and a traceless imaginary part.

The properties of the trace of the complex 1-particle density matrix are very similar to those of a real Hermitian density matrix. As such, it allows for similar kinds analysis. In particular, the complex difference density can be decomposed into complex attachment and detachment densities[50] that can be visualized to give a picture of both the electron-attached state and the polarization of the target. The difference density

$$\mathbf{\Delta} = \mathbf{P}^{\mathrm{res}} - \mathbf{P}^{\mathrm{tar}} \tag{14}$$

is defined as the difference between the complex electron density of the resonance and the real density of the target. This quantity can be uniquely decomposed by splitting its eigenvalues into those with positive real part and those with negative real part:

$$\mathbf{\Delta} = \mathbf{U}(\mathbf{a} - \mathbf{d})\mathbf{U}^{\mathrm{T}} = \mathbf{A} - \mathbf{D} \tag{15}$$

where $\mathbf{a}$ and $\mathbf{d}$ are diagonal matrices with positive real parts. $\mathbf{A}$ and $\mathbf{D}$ are termed the attachment and detachment densities respectively. These quantities describe the electron density and the hole density of the resonance relative to the target. Furthermore, the eigenvalues of these two matrices are related to the scattering process in that

$$\mathrm{Tr}(\mathbf{A}) - \mathrm{Tr}(\mathbf{D}) = \mathrm{Tr}(\mathbf{\Delta}) = n \tag{16}$$

where n is the number of electrons in the resonance state relative to the target; $n = 1$ for an anion resonance. Therefore, the two equivalent quantities

$$\mathrm{Tr}(\mathbf{A}) - n \quad \text{and} \quad \mathrm{Tr}(\mathbf{D}) \tag{17}$$

provide a measure of the magnitude of the polarization.

Two-electron properties can be expressed in terms of the 2-particle density matrix, but the only two-electron property relevant in this study is the square of the total spin which can be computed as[51]

$$\langle S^2 \rangle = \left(\frac{N_\alpha - N_\beta}{2} \right) \left(\frac{N_\alpha - N_\beta}{2} + 1 \right) + N_\beta - \sum_{ij}^{\mathrm{occ}} (i_\alpha | j_\beta)^2 \tag{18}$$

where N_α and N_β are the numbers of α and β electrons respectively. For spin-pure wavefunctions such as the NH-ROHF wavefunction, the expectation value of total spin squared is real and equal to $s(s+1)$ where s is the total spin quantum number. For NH-UHF wavefunctions, the expectation value can vary from the spin-pure value and can develop an imaginary part. As in the Hermitian case, the computation of the square of the total spin provides a measure of the spin contamination of the unrestricted wavefunction. In practice, the expectation value of S^2 is computed for each value of θ and the rational interpolation scheme described in Ref. 10 was used to compute the expectation value at the optimal value of θ.

III. RESULTS

All computations reported in this study were performed with a modified version of the Q-Chem software package.[52] Matrix elements were computed by the methods described in Ref. 10, while the Armadillo C++ linear algebra library[53] was used for all matrix manipulations. All SCF calculations are converged to the extent that the maximum element of the (orthogonalized) DIIS error is less than 10^{-5}.

A. Small molecules and comparison to static exchange

Table I shows the computed Siegert energies of low energy shape resonances in four different molecular systems and in three basis sets of increasing size. The geometries are

molecule	basis	SE[a]		NH-ROHF		NH-UHF		$\langle S^2 \rangle$	
		Re[E]	Im[E]	Re[E]	Im[E]	Re[E]	Im[E]	Re[$\langle S^2 \rangle$]	Im[$\langle S^2 \rangle$]
N_2	caug-cc-pVDZ(cm+)	3.9752	-0.6363	2.9517	-0.1566	2.8366	-0.1087	0.7580	-0.0044
	caug-cc-pVTZ(cm+)	3.8818	-0.6301	2.9621	-0.1613	2.8287	-0.1159	0.7594	-0.0049
	caug-cc-pVQZ(cm+)	3.8413	-0.6215	2.9525	-0.1547	2.8271	-0.1078	0.7590	-0.0041
CO	caug-cc-pVDZ(cm+)	3.4173	-0.9715	2.5253	-0.3463	2.4304	-0.2814	0.7568	-0.0015
	caug-cc-pVTZ(cm+)	3.3474	-0.9407	2.4124	-0.3185	2.4216	-0.2879	0.7570	-0.0020
	caug-cc-pVQZ(cm+)	3.3441	-0.9646	2.5423	-0.3534	2.4263	-0.3032	0.7574	-0.0020
CO_2	caug-cc-pVDZ(cm+)	5.5268	-0.2972	4.4207	-0.0175	4.0296	0.0302	0.7620	-0.0007
	caug-cc-pVTZ(cm+)	5.5035	-0.3435	4.4625	-0.0677	4.3096	-0.0516	0.7639	-0.0012
	caug-cc-pVQZ(cm+)	5.4733	-0.3500	4.4553	-0.0677	4.3111	-0.0559	0.7638	-0.0011
CH_2O	caug-cc-pVDZ(cm+)	2.6848	-0.8078	1.7544	-0.2245	1.6251	-0.1676	0.7613	-0.0064
	caug-cc-pVTZ(cm+)	2.6459	-0.7887	1.7861	-0.2012	1.6472	-0.1541	0.7624	-0.0063
	caug-cc-pVQZ(cm+)	2.5775	-0.8170	1.7467	-0.2007	1.6132	-0.1409	0.7623	-0.0065

[a] Also reported in Ref. 10

TABLE I. Positions and widths in eV of the lowest $^2\Pi_g$ resonance in N_2 and CO, the lowest $^2\Pi_u$ resonance in CO_2 and the lowest $^2B_1$ shape resonance in formaldehyde (CH_2O). Expected values of total spin-squared are reported for the NH-UHF calculations. The basis sets are described in detail in Ref. 10.

molecule	geometry
N_2	N≡N = 1.094Å
CO	C≡O = 1.128Å
CO_2	C=O = 1.16Å
CH_2O	C-H = 1.11Å, C=O = 1.205Å, H-C-H = 116.2°

TABLE II. Geometries used throughout the present study.

reported in Table II. The positions from NH-SCF calculations are reported relative to the total Hermitian RHF energy of the target in the same basis ($\theta = 0°$). The positions and widths are computed at the NH-UHF and NH-ROHF levels of theory and are compared to the SE results in the same basis sets. A recent summary of previous theoretical and experimental positions and widths for these resonances can be found in Ref. 54. In general, the positions computed with NH-ROHF are $0.9-1$eV lower in energy than the corresponding SE result. The positions computed with NH-UHF are $1-1.1$eV lower in energy than the SE result making them on average about 0.1eV lower in energy than the corresponding NH-ROHF result. This is as expected; the extra polarization terms in the UHF wavefunction should lower the position relative to the energy of the neutral target.

The widths are not so predictable. We would expect the widths from NH-SCF calculations to be significantly smaller than for SE calculations due to the incorporation of polarization. This effect is indeed observed, but the magnitude of the difference is not as constant among different molecular systems. For similar reasons, the widths computed with NH-UHF would be expected to be lower than those computed with NH-ROHF, and this is generally the case.

The behavior of the Siegert energies as size of the basis is increased is also generally difficult to predict. However, despite a couple of exceptions, both the real and imaginary parts of the energy are relatively stable with respect to an increase in the size of the basis. The first exception is the Π_u resonance in CO_2 computed within the caug-cc-pVDZ(cm+) basis set. In this case, the positions are reasonable, but the computed widths are unreasonably small; the NH-UHF energy has a positive imaginary part. However, this case is a pathological one in that the basis set contains exactly one complex function of π_u symmetry. This grossly incomplete basis cannot be expected to yield an accurate width, and it is quite surprising that the SE result is so reasonable. A more detailed discussion of basis set effects can be found in Ref. 10. The other slight exception is the Π_g resonance in carbon monoxide as computed with NH-ROHF in the caug-cc-pVTZ(cm+) basis set. Both the position and width computed in this basis set differ from their values computed in the larger and smaller basis sets. The reason for this slight deviation is unknown.

We also report the expectation values of total spin-squared for the NH-UHF wavefunctions in Table I. The real parts of the spin-squared values are comparable to what would be expected from a Hermitian calculation on a bound anion in that they are only slightly different from the pure doublet, while the imaginary parts are quite small. This suggests

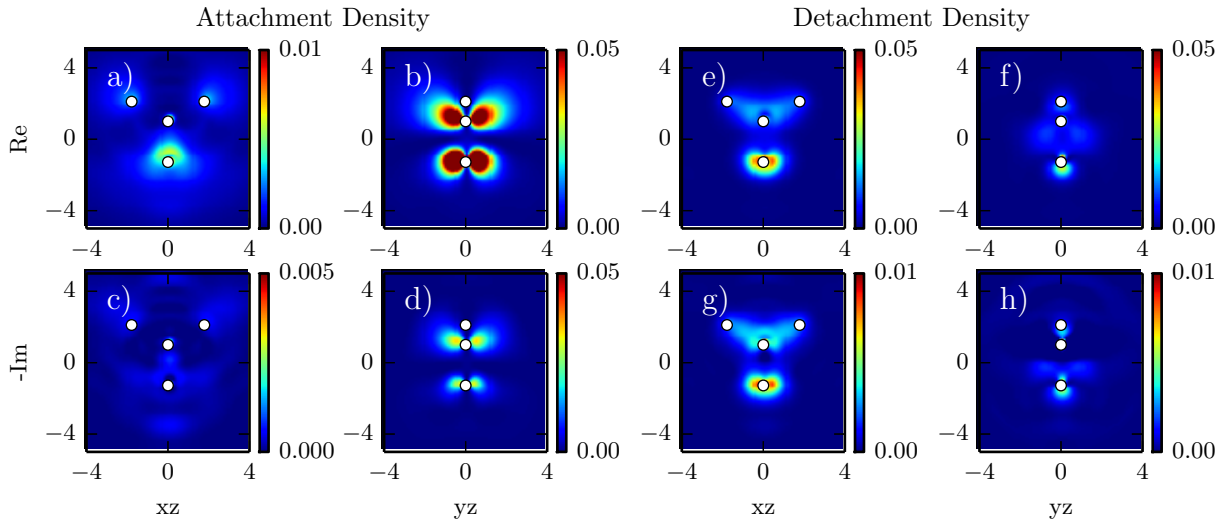

FIG. 2. Real and imaginary parts of the α attachment and detachment densities for the $^2B_1$ resonance in formaldehyde are plotted in the xz and yz-planes. The top row shows the real part and the bottom row shows the negative of the imaginary part. The first four panels (a - d) show the attachment density while the second four (e - h) show the detachment density. Note the difference in scales. White dots are used to indicate the positions of the nuclear centers; the oxygen end of the molecule points in the negative z-direction. The axes are in atomic units (a_0). The real and imaginary parts of the attachment density, which correspond to the extra electron in the resonance state, are predominantly π^* in character. The detachment density, which corresponds to rearrangement, has largely σ character.

that for these cases, the unrestricted wavefunction is not significantly spin-contaminated.

Comparing to other theoretical and experimental results is difficult to do systematically because of the wide range of methods/basis sets and experimental conditions. However, the results presented here qualitatively reproduce the experimental numbers and agree with many other theoretical results (*cf.* Ref. 54). Some selected literature values are shown in Table III. In general, we can say that the positions are larger than those computed with correlated methods. The widths fall within the range of other theoretical results, but seem to be slightly smaller on average than widths computed at similar levels of theory.

molecule	method	position	width
N_2	Stieltjes imaging[55]	2.23	0.40
	Schwinger variational + ADC(3) optical potential[56]	2.534	0.536
	NH-SCF with complex basis functions[11]	3.19	0.44
	3rd order decouplings of dilated electron propogator[57]	2.11	0.18
	EOM-EA-CCSD stabilization (aug-cc-pV5Z)[58]	2.49	0.248
	CAP EOM-EA-CCSD (1st order, aug-cc-pVQZ + 3s3p3d)[54]	2.478	0.286
	Experimental estimate[59]	2.32	0.41
CO	T-matrix (static-exchange)[60]	3.4	1.65
	2nd order electron propogator[61]	1.71	0.08
	3rd order decouplings of the electron propogator[57]	1.65	0.14
	CAP EOM-EA-CCSD (1st order, aug-cc-pV5Z + 3s3p3d)[54]	1.762	0.604
	Experimental estimate[62]	1.50	0.4
CO_2	Schwinger variational (static-exchange)[63]	5.39	0.64
	Schwinger variational (static-exchange + polarization)[64]	3.78	0.23
	CAP EOM-EA-CCSD (1st order, aug-cc-pVTZ + 3s3p3d)[54]	3.997	0.198
	Experiment[65]	3.14	0.20
CH_2O	Complex Kohn (static-exchange + polarization)[66]	1.0	∼0.5
	2nd order decouplings of the dilated electron propogator (largest basis)[67]	0.887	0.076
	R-matrix (static-exchange + polarization)[68]	1.32	0.546
	CAP EOM-EA-CCSD (1st order, aug-cc-pVTZ + 3s3p3d)[54]	1.314	0.277
	Experiment[69]	∼0.86	-

TABLE III. Selected literature values (in eV) for the resonances studied here from experiment and various levels of theory.

B. Density based analysis of formaldehyde's B_1 resonance

In this section, the attachment and detachment densities of the $^2B_1$ resonance in formaldehyde are computed at the optimal value of θ in the caug-cc-pVTZ basis. Because the c-norm does not permit a rigorous notion of matrix positivity, there are in general no restrictions

	Attachment		Detachment	
	Re	Im	Re	Im
α	1.3233	-0.0391	0.3233	-0.0391
β	0.3905	-0.1140	0.3905	-0.1140

TABLE IV. Traces of attachment and detachment densities for the α and β difference densities corresponding to the B_1 resonance in formaldehyde. The densities were computed at the optimal value of θ in the caug-cc-pVTZ(cm+) basis set.

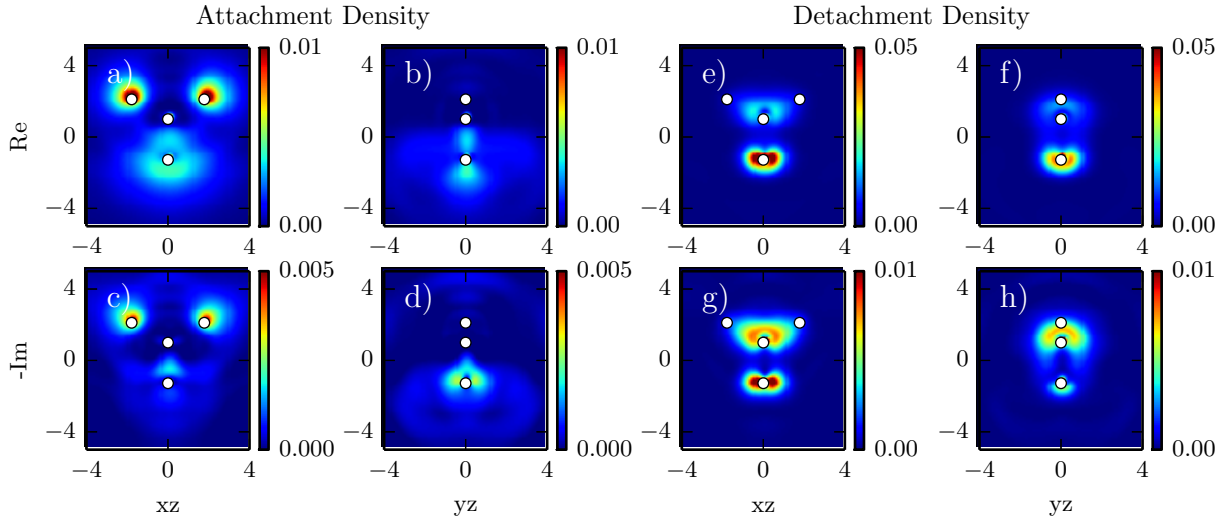

FIG. 3. Real and imaginary parts of the β attachment and detachment densities for the $^2B_1$ resonance in formaldehyde are plotted in the xz and yz-planes. The top row shows the real part and the bottom row shows the negative of the imaginary part. The first four panels (a - d) show the attachment density while the second four (e - h) show the detachment density. Note the differences in scales. White dots are used to indicate the positions of the nuclear centers; the oxygen end of the molecule points in the negative z-direction. The axes are in atomic units (a_0). All changes in the β space are due to electron-rearrangement which is mostly of σ character.

on the signs of the real and imaginary parts of these densities, though the real parts are generally observed to be mostly positive while imaginary parts are observed to be primarily negative.

The attachment and detachment densities, by definition, obey the relations of Equa-

tion 17. This is confirmed in Table IV where the real and imaginary parts of the traces of the attachment and detachment densities are shown. Note that the attached electron has α spin in this case. These values provide an approximate, but quantitative, description of the polarization during the electron attachment process: approximately 0.32 α electrons and 0.39 β electrons are rearranged. The larger polarization of the β density is consistent with the nature of the exchange interaction.

The α and β attachment and detachment densities for formaldehyde's B_1 resonance are plotted in Figures 2 and 3 respectively. Note that it is the negative of the imaginary part that is plotted in the bottom rows of Figures 2 and 3 (c,d,g,h). The real part of the α attachment density has very little magnitude in the plane of the molecule and therefore resembles the density arising from attachment to a state with π character. The small σ character in the attachment density is likely the result of electron rearrangement.

Comparing the β attachment and detachment densities, it is clear that the rearrangement in the β space involves the movement of electron density from orbitals localized around the oxygen atom to the two hydrogen atoms. It is also interesting to note that the β attachment density is significantly delocalized in comparison with the detachment density.

C. A_1 and T_2 resonances in carbon tetrafluoride

Carbon tetrafluoride has been observed to have two low energy shape resonances of A_1 and T_2 symmetry. These two resonances have been the subject of some recent interest due to their role in dissociative electron attachment.[76–78] Computed positions and widths of these two shape resonances are shown in Table V. The positions and widths computed at the SE, NH-ROHF, and NH-UHF levels of theory are shown along with literature values from various theoretical calculations. The spin-squared values for the UHF wavefunctions are shown in Table VI and a summary of experimental results can be found in Refs. 79,80.

This case is interesting in that the NH-ROHF and NH-UHF values agree quite closely. The spin squared values (shown in Table VI) show that there is very little spin contamination in the NH-UHF wavefunction, but the similarity is still quite striking when compared to similar calculations on small molecules. Furthermore, while the positions calculated with NH-UHF are smaller than those computed with NH-ROHF, the widths are slightly larger in several cases. This is contrary to the trends observed in other molecules, though it is in

reference	T_2 resonance		A_1 resonance		method
	Position	Width	Position	Width	
Huo[70]	6.6	4.1	11.7	22.8	Schwinger Variational(SE)
Modelli et al[71]	8.95	-	8.70	-	Multiple Scattering-Xα
Modelli et al[71]	8.58	-	8.98	-	Continuum Multiple Scattering-Xα
Winstead et al[72]	11.5	-	13.0	-	Schwinger Multichannel (SE)
Isaacson et al[73]	$\sim 9^a$	-	$\sim 9^a$	-	Complex Kohn
Curik et al[74]	$8-10^a$	-	$8-10^a$	-	Close-coupling (model potential)
Varella et al[75]	9.9	-	11.0	-	Schwinger Multichannel (SEP)
present work[b]	10.6301	2.0553	12.7184	2.0902	SE/caug-cc-pVDZ
present work[b]	11.0816	1.9737	12.0561	1.9617	SE/caug-cc-pVTZ
present work	8.6421	0.8530	9.7906	1.8189	NH-ROHF/caug-cc-pVDZ
present work	9.0738	0.7813	10.0711	1.1740	NH-ROHF/caug-cc-pVTZ
present work	8.5996	0.9139	9.5236	1.8346	NH-UHF/caug-cc-pVDZ
present work	8.8851	0.8191	9.9862	1.1490	NH-UHF/caug-cc-pVTZ

TABLE V. Calculated positions and widths (eV) of low energy shape resonances in CF_4. Static-exchange plus polarization is abbreviated SEP.

[a] overlapping resonances not separately resolved

[b] Also reported in Ref. 10

resonance	basis	$\langle S^2 \rangle$	
		$\mathrm{Re}[\langle S^2 \rangle]$	$\mathrm{Im}[\langle S^2 \rangle]$
	caug-cc-pVDZ(cm+)	0.7542	-0.0032
A_1	caug-cc-pVTZ(cm+)	0.7551	-0.0017
	caug-cc-pVDZ(cm+)	0.7515	-0.0010
T_2	caug-cc-pVTZ(cm+)	0.7588	-0.0018

TABLE VI. Spin-squared of the A_1 and T_2 shape resonances in CF_4 computed using NH-UHF.

no way prohibited by the theory.

For these resonances in CF_4, like those of many polyatomic molecules, very few *ab initio* calculations have been performed. The results of the present study agree well with the previous theoretical results shown in Table V excluding the calculation of Huo.[70] Though Huo is the only author to report a width, all other studies report the computed cross-section which shows the widths of the two, not always resolveable, resonances to be on the order of 1eV which agrees well with the present study. The results presented here offer the most complete picture of these two resonances: the T_2 resonance clearly appears approximately 1eV lower energy and with a slightly narrower width, though both widths are on the order of 1eV. It is possible that this picture is significantly different when electron-correlation is explicitly included in the theory.

D. Carbon monoxide potential energy curve

One of the great attractions of Hermitian UHF theory is that, in many situations, it provides a qualitatively correct description of dissociation processes. NH-UHF theory should be able to describe potential energy curves of resonances with the same qualitative accuracy.

As an example, we examine the potential energy curves of anionic and neutral carbon monoxide at the NH-UHF and UHF level of theory respectively. The anion, metastable at the equilibrium geometry of the neutral, becomes bound as the molecule is stretched, eventually dissociating to oxygen neutral and carbon anion.

The potential energy curves at the UHF/NH-UHF level of theory are shown in Figure 4. The behavior is qualitatively what would be expected: the anion curve crosses that of the neutral and the width goes to zero. However, the point at which the width goes to zero occurs about 0.1Å before the curves cross. This is consistent with previous calculations[12,13] and typical of cases where the same uncorrelated level of theory is used on the closed-shell neutral and open-shell anion. Higher levels of theory may be able to remove this discrepancy.[81] In the region where the anion is bound, the NH-UHF energy almost exactly reproduces the Hermitian UHF energy of the bound anion, but with a very small positive imaginary part. In the region where the anion is unbound and Hermitian UHF is not useful, NH-UHF provides a qualitatively correct complex potential. Such complex potential curves could be useful in calculations of vibrational structure in electron scattering experiments.[82–84]

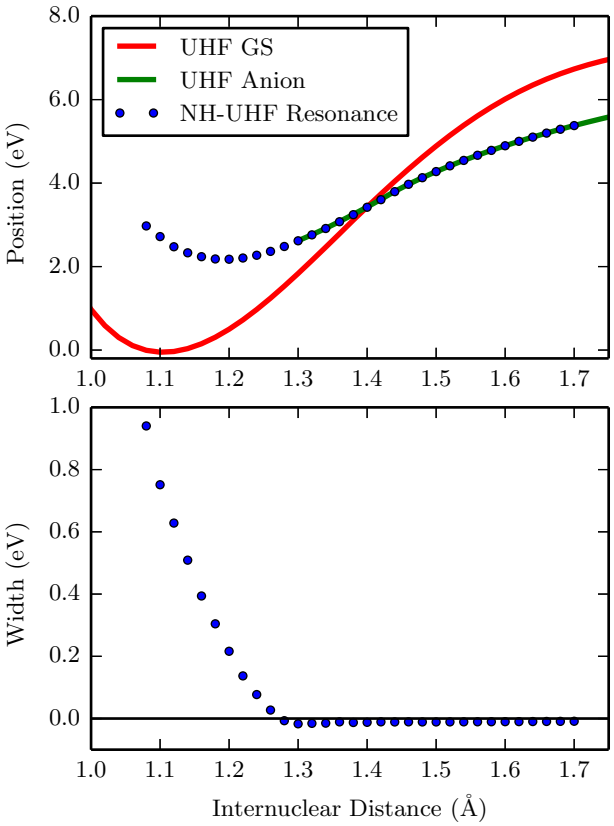

FIG. 4. Carbon monoxide potential energy curves at the UHF/NH-UHF level of theory in the caug-cc-pVTZ(cm+) basis set.

The real and imaginary parts of the expectation value of total spin squared are plotted in Figure 5. In this case, the Hermitian UHF solution was obtainable throughout the recoupling region. The expectation value of total spin-squared of the NH-UHF agrees remarkably well with that of the Hermitian UHF solution. This is not surprising, because the anion is bound for much of this region. It is, however, worthy of note that the NH-UHF does essentially reproduce the Hermitian UHF solution in the region where the width is zero.

This potential energy curve was not easy to obtain. Only by reading in orbitals from previous calculations and taking small (0.02Å) steps in internuclear distance and similarly small (0.5°) steps in θ was convergence achieved at enough points so that the analytic continuation scheme could be confidently applied. Also, at some geometries multiple stationary points were observed, and great care had to be taken to make sure that we followed a single stationary solution.

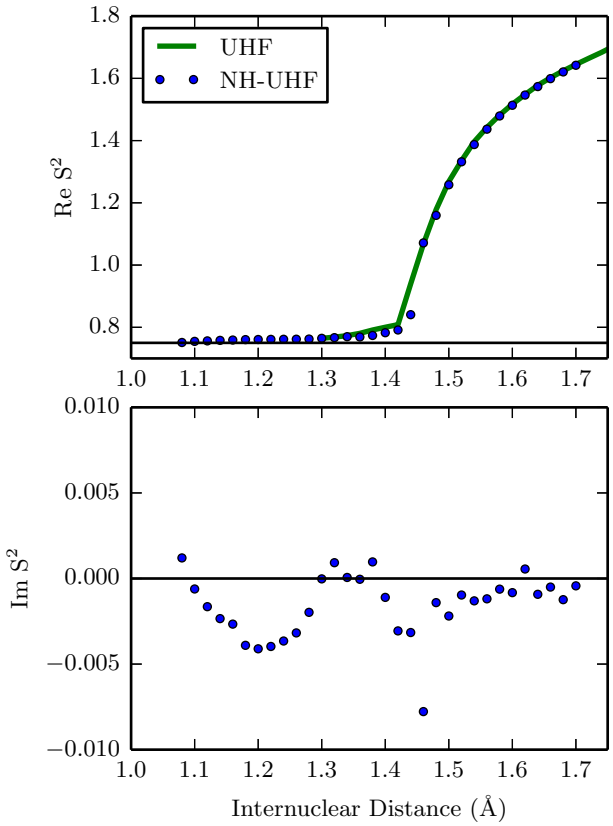

FIG. 5. Total spin squared on the carbon monoxide PES in the caug-cc-pVTZ(cm+) basis set. The black line indicates a pure doublet.

IV. CONCLUSIONS

In this study complex basis functions were employed in the implementation of the NH-ROHF method, and the novel NH-UHF method. These methods were described in detail and applied to a variety of small diatomic and polyatomic molecules including carbon tetrafluoride. The computation and interpretation of molecular properties from non-Hermitian wavefunctions was discussed and a density-based analysis was applied to the $^2B_1$ resonance in formaldehyde. This analysis of the complex analogs of the attachment and detachment densities allows for an intuitive discussion of target polarization during the process of resonant electron attachment. The NH-UHF method was also utilized in the computation of a NH-UHF potential energy surface for the metastable carbon monoxide anion. These promising results make it worth investigating the possibility of using an NH-SCF reference for highly accurate correlated calculations on small molecules.

However, it is also important to be aware that there are significant challenges in extending NH-SCF methods to larger systems than reported here. First, NH-SCF with complex basis functions often suffers from slow convergence. Second, there are serious numerical problems associated with linear dependence in very large basis sets, associated for instance with diffuse complex Gaussians on multiple atomic centers. Third, the occasional appearance of multiple stationary points can make the identification of the Siegert energy ambiguous, though we have not yet seen a case where the difference is significant. Finally, the θ-trajectories are a significant burden relative to conventional SCF. More effort is necessary to remedy these problems so that the method can be applied confidently to large molecules.

ACKNOWLEDGMENTS

Support for this work was provided through the Scientific Discovery through Advanced Computing (SciDAC) program funded by the U.S. Department of Energy, Office of Science, Advanced Scientific Computing Research, and Basic Energy Sciences. The authors thank Satoshi Yabushita for providing valuable computational benchmarks using an independent complex Gaussian implementation based on the COLUMBUS quantum chemistry codes. The authors thank Paul Horn for invaluable advice on the implementation of non-linear solvers.

REFERENCES

[1]B. Junker, Advances in Atomic and Molecular Physics **18**, 207 (1982).

[2]W. Reinhardt, Annu. Rev. Phys. Chem. **33**, 223 (1982).

[3]N. Moiseyev, Phys. Rep. **302**, 211 (1998).

[4]J. Aguilar and J. Combes, Commun. Math. Phys. **22**, 269 (1971).

[5]E. Balslev and J. Combes, Commun. Math. Phys. **22**, 280 (1971).

[6]B. Simon, Commun. Math. Phys. **27**, 1 (1972).

[7]C. McCurdy and T. Rescigno, Phys. Rev. Lett. **41**, 1364 (1978).

[8]B. Simon, Phys. Lett. A **71A**, 211 (1979).

[9]J. Morgan and B. Simon, J. Phys. B: At., Mol. Opt. Phys. **14**, L167 (1981).

[10]A. F. White, M. Head-gordon, and C. W. Mccurdy, J. Chem. Phys. **142**, 054103 (2015).

[11]T. Rescigno, A. Orel, and C. W. McCurdy, J. Chem. Phys. **73**, 6347 (1980).

[12]C. W. McCurdy and R. Mowrey, Phys. Rev. A **25**, 2529 (1982).

[13]J. G. Lauderdale, C. W. McCurdy, and A. U. Hazi, J. Chem. Phys. **79**, 2200 (1983).

[14]S. Yabushita and C. W. McCurdy, J. Chem. Phys. **83**, 3547 (1985).

[15]M. Honigmann, G. Hirsch, R. J. Buenker, I. D. Petsalakis, and G. Theodorakopoulos, Chem. Phys. Lett. **305**, 465 (1999).

[16]M. Honigmann, R. J. Buenker, and H.-P. Liebermann, J. Chem. Phys. **125**, 234304 (2006).

[17]M. Honigmann, R. J. Buenker, and H.-P. Liebermann, J. Chem. Phys. **131**, 034303 (2009).

[18]M. Honigmann, R. J. Buenker, and H.-P. Liebermann, J. Comput. Chem. **33**, 355 (2012).

[19]C. W. McCurdy, T. N. Rescigno, E. R. Davidson, and J. G. Lauderdale, J. Chem. Phys. **73**, 3268 (1980).

[20]M. Mishra, Y. Öhrn, and P. Froelich, Phys. Lett. A **84**, 4 (1981).

[21]C. W. McCurdy, J. G. Lauderdale, and R. Mowrey, J. Chem. Phys. **75**, 1835 (1981).

[22]J. McNutt and C. W. McCurdy, Phys. Rev. A **27**, 132 (1983).

[23]D. Frye and L. Armstrong, Phys. Rev. A **34**, 1682 (1986).

[24]M. Bentley, Phys. Rev. A **42**, 3826 (1990).

[25]D. Whitenack and A. Wasserman, Phys. Rev. Lett. **107**, 163002 (2011), arXiv:arXiv:1106.3911v1.

[26]Y. Zhou and M. Ernzerhof, J. Phys. Chem. Lett. **3**, 1916 (2012).

[27]Y. Zhou and M. Ernzerhof, J. Chem. Phys. **136**, 094105 (2012).

[28]A. H. Larsen, U. De Giovannini, D. L. Whitenack, A. Wasserman, and A. Rubio, J. Phys. Chem. Lett. **4**, 2734 (2013).

[29]D. L. Yeager and M. K. Mishra, Int. J. Quantum Chem. **104**, 871 (2005).

[30]K. Samanta and D. L. Yeager, Int. J. Quantum Chem. **110**, 798 (2010).

[31]P. R. Žd'Ánská and N. Moiseyev, J. Chem. Phys. **123** (2005), 10.1063/1.2110169.

[32]S. B. Zhang and D. L. Yeager, J. Mol. Struct. **1023**, 96 (2012).

[33]S. B. Zhang and D. L. Yeager, Phys. Rev. A **85**, 032515 (2012).

[34]K. B. Bravaya, D. Zuev, E. Epifanovsky, and A. I. Krylov, J. Chem. Phys. **138**, 124106 (2013).

[35]Y. Sajeev, a. Ghosh, N. Vaval, and S. Pal, Int. Rev. Phys. Chem. **33**, 397 (2014).

[36]E. Brändas and P. Froelich, Phys. Rev. A **16**, 2207 (1977).

[37]N. Moiseyev, P. Certain, and F. Weinhold, Mol. Phys. **36**, 1613 (1978).

[38]N. Moiseyev, Mol. Phys. **47**, 585 (1982).

[39]C. Roothaan, Rev. Mod. Phys. **32**, 179 (1960).

[40]E. Davidson and L. Stenkamp, Int. J. Quantum Chem. **31**, 21 (1976).

[41]B. N. Plakhutin, E. V. Gorelik, and N. N. Breslavskaya, J. Chem. Phys. **125**, 204110 (2006).

[42]J. a. Pople and R. K. Nesbet, J. Chem. Phys. **22**, 571 (1954).

[43]F. E. Harris and H. a. Pohl, J. Chem. Phys. **42**, 3648 (1965).

[44]D. W. Small, E. J. Sundstrom, and M. Head-Gordon, J. Chem. Phys. **142**, 024104 (2015).

[45]A. T. B. Gilbert, N. a. Besley, and P. M. W. Gill, J. Phys. Chem. A **112**, 13164 (2008).

[46]P. Pulay, Chem. Phys. Lett. **73**, 393 (1980).

[47]P. Pulay, J. Comput. Chem. **3**, 556 (1982).

[48]L. Schlessinger, Phys. Rev. **36**, 1411 (1968).

[49]P. Pulay, Mol. Phys. **17**, 197 (1969).

[50]M. Head-Gordon, A. M. Grana, D. Maurice, and C. a. White, J. Phys. Chem. **99**, 14261 (1995).

[51]A. Szabo and N. Ostlund, Modern Quantum Chemistry (McGraw-Hill, 1982) p. 107.

[52]Y. Shao, Z. Gan, E. Epifanovsky, A. T. Gilbert, M. Wormit, J. Kussmann, A. W. Lange, A. Behn, J. Deng, X. Feng, D. Ghosh, M. Goldey, P. R. Horn, L. D. Jacobson, I. Kaliman, R. Z. Khaliullin, T. Kuś, A. Landau, J. Liu, E. I. Proynov, Y. M. Rhee, R. M. Richard, M. a. Rohrdanz, R. P. Steele, E. J. Sundstrom, H. L. Woodcock, P. M. Zimmerman, D. Zuev, B. Albrecht, E. Alguire, B. Austin, G. J. O. Beran, Y. a. Bernard, E. Berquist, K. Brandhorst, K. B. Bravaya, S. T. Brown, D. Casanova, C.-M. Chang, Y. Chen, S. H. Chien, K. D. Closser, D. L. Crittenden, M. Diedenhofen, R. a. DiStasio, H. Do, A. D. Dutoi, R. G. Edgar, S. Fatehi, L. Fusti-Molnar, A. Ghysels, A. Golubeva-Zadorozhnaya, J. Gomes, M. W. Hanson-Heine, P. H. Harbach, A. W. Hauser, E. G. Hohenstein, Z. C. Holden, T.-C. Jagau, H. Ji, B. Kaduk, K. Khistyaev, J. Kim, J. Kim, R. a. King, P. Klunzinger, D. Kosenkov, T. Kowalczyk, C. M. Krauter, K. U. Lao, A. Laurent, K. V. Lawler, S. V. Levchenko, C. Y. Lin, F. Liu, E. Livshits, R. C. Lochan, A. Luenser, P. Manohar, S. F. Manzer, S.-P. Mao, N. Mardirossian, A. V. Marenich, S. a. Maurer, N. J. Mayhall, E. Neuscamman, C. M. Oana, R. Olivares-Amaya, D. P. ONeill, J. a. Parkhill, T. M. Perrine, R. Peverati, A. Prociuk, D. R. Rehn, E. Rosta, N. J. Russ, S. M. Sharada, S. Sharma, D. W. Small, A. Sodt, T. Stein, D. Stück, Y.-C. Su, A. J. Thom, T. Tsuchi-

mochi, V. Vanovschi, L. Vogt, O. Vydrov, T. Wang, M. a. Watson, J. Wenzel, A. White, C. F. Williams, J. Yang, S. Yeganeh, S. R. Yost, Z.-Q. You, I. Y. Zhang, X. Zhang, Y. Zhao, B. R. Brooks, G. K. Chan, D. M. Chipman, C. J. Cramer, W. a. Goddard, M. S. Gordon, W. J. Hehre, A. Klamt, H. F. Schaefer, M. W. Schmidt, C. D. Sherrill, D. G. Truhlar, A. Warshel, X. Xu, A. Aspuru-Guzik, R. Baer, A. T. Bell, N. a. Besley, J.-D. Chai, A. Dreuw, B. D. Dunietz, T. R. Furlani, S. R. Gwaltney, C.-P. Hsu, Y. Jung, J. Kong, D. S. Lambrecht, W. Liang, C. Ochsenfeld, V. a. Rassolov, L. V. Slipchenko, J. E. Subotnik, T. Van Voorhis, J. M. Herbert, A. I. Krylov, P. M. Gill, and M. Head-Gordon, Mol. Phys. **113**, 184 (2014).

[53]C. Sanderson, "Armadillo: An open source C++ linear algebra library for fast prototyping and computationally intensive experiments," Tech. Rep. (NICTA, 2010).

[54]D. Zuev, T.-C. Jagau, K. B. Bravaya, E. Epifanovsky, Y. Shao, E. Sundstrom, M. Head-Gordon, and A. I. Krylov, J. Chem. Phys. **141**, 024102 (2014).

[55]a. Hazi, T. Rescigno, and M. Kurilla, Phys. Rev. A **23**, 1089 (1981).

[56]H.-D. Meyer, Phys. Rev. A **40**, 5605 (1989).

[57]S. Mahalakshmi, A. Venkatnathan, and M. K. Mishra, J. Chem. Phys. **115**, 4549 (2001).

[58]M. F. Falcetta, L. A. Difalco, D. S. Ackerman, J. C. Barlow, and K. D. Jordan, J. Phys. Chem. A **118**, 7489 (2014).

[59]M. Berman, H. Estrada, L. S. Cederbaum, and W. Domcke, Phys. Rev. A **28**, 1363 (1983).

[60]D. A. Levin, A. W. Fliflet, and V. McKoy, Phys. Rev. A **21**, 1202 (1980).

[61]R. a. Donnelly, Int. J. Quantum Chem. **28**, 363 (1985).

[62]H. Ehrhardt, L. Langhans, F. Linder, and H. S. Taylor, Phys. Rev. **173**, 222 (1968).

[63]R. R. Lucchese and V. McKoy, Phys. Rev. A **25**, 1963 (1982).

[64]C.-H. Lee, C. Winstead, and V. McKoy, J. Chem. Phys. **111**, 5056 (1999).

[65]L. Sanche and G. Schulz, J. Chem. Phys. **58**, 479 (1973).

[66]T. Rescigno, C. W. McCurdy, and B. Schneider, Phys. Rev. Lett. **63**, 248 (1989).

[67]S. Mahalakshmi and M. Mishra, Chem. Phys. Lett. **296**, 43 (1998).

[68]S. Kaur and K. L. Baluja, J. Phys. B: At., Mol. Opt. Phys. **38**, 3917 (2005).

[69]C. Benoit and R. Abouaf, Chem. Phys. Lett. **123**, 134 (1986).

[70]W. M. Huo, Phys. Rev. A **38**, 3303 (1988).

[71]A. Modelli, F. Scagnolari, G. Distefano, D. Jones, and M. Guerra, J. Chem. Phys. **96**, 2061 (1992).

[72]C. Winstead, Q. Sun, and V. McKoy, J. Chem. Phys. **98**, 1105 (1993).

[73]W. Isaacs, C. McCurdy, and T. Rescigno, Phys. Rev. A **58**, 309 (1998).

[74]R. Curik, F. a. Gianturco, and N. Sanna, J. Phys. B: At., Mol. Opt. Phys. **33**, 615 (2000).

[75]M. Varella, C. Winstead, V. McKoy, M. Kitajima, and H. Tanaka, Phys. Rev. A **65**, 022702 (2002).

[76]E. H. Bjarnason, F. H. Ómarsson, M. Hoshino, H. Tanaka, M. J. Brunger, P. Limão Vieira, and O. Ingólfsson, Int. J. Mass Spectrom. **339-340**, 45 (2013).

[77]L. Xia, X.-J. Zeng, H.-K. Li, B. Wu, and S. X. Tian, Angew. Chem. **125**, 1047 (2013).

[78]F. H. Ómarsson, E. Szymanska, N. J. Mason, E. Krishnakumar, and O. Ingólfsson, Phys. Rev. Lett. **111**, 063201 (2013).

[79]L. G. Christophorou, J. K. Olthoff, and M. V. V. S. Rao, J. Phys. Chem. Ref. Data **25**, 1341 (1996).

[80]J. S. Yoon, M. Y. Song, H. Kato, M. Hoshino, H. Tanaka, M. J. Brunger, S. J. Buckman, and H. Cho, J. Phys. Chem. Ref. Data **39** (2010), 10.1063/1.3475647.

[81]T.-c. Jagau and A. I. Krylov, J. Phys. Chem. Lett. **5**, 3078 (2014).

[82]A. Herzenberg, Journal of Physics B **1**, 548 (1968).

[83]L. Dubé and a. Herzenberg, Phys. Rev. A **20**, 194 (1979).

[84]C. W. McCurdy, J. Chem. Phys. **78**, 6773 (1983).

Appendix A: Optimal theta values

Optimal values of the scaling factor for all single point energy calculations are provided in Table VII. The optimal values for the carbon monoxide PES are shown in Table VIII. Note that the scaling factor is defined as

$$s \equiv e^{i\theta}.$$

molecule	basis	SE		NH-ROHF		NH-UHF	
		$\|s\|$	phase[s]	$\|s\|$	phase[s]	$\|s\|$	phase[s]
	caug-cc-pVDZ(cm+)	1.0989	20.864	1.0187	13.746	1.0338	10.930
N_2	caug-cc-pVTZ(cm+)	0.9604	23.427	0.9787	9.7308	0.9620	8.8183
	caug-cc-pVQZ(cm+)	1.1052	21.120	1.0005	9.0439	0.9989	12.264
	caug-cc-pVDZ(cm+)	0.9638	25.628	0.9310	19.862	0.9544	14.889
CO	caug-cc-pVTZ(cm+)	1.0264	23.195	0.9935	25.186	0.9518	11.023
	caug-cc-pVQZ(cm+)	1.0167	27.888	0.9855	17.874	1.0126	17.255
	caug-cc-pVDZ(cm+)	0.9067	10.560	1.0010	14.383	1.0043	17.380
CO_2	caug-cc-pVTZ(cm+)	1.0687	19.233	1.0654	14.960	1.0720	15.507
	caug-cc-pVQZ(cm+)	1.0025	20.992	0.9208	25.423	1.0284	14.639
	caug-cc-pVDZ(cm+)	1.0359	23.459	0.9934	19.944	0.9938	19.765
CH_2O	caug-cc-pVTZ(cm+)	0.9742	18.154	1.0790	4.799	1.0626	17.062
	caug-cc-pVQZ(cm+)	1.0880	26.177	1.0021	22.736	1.0227	24.807
	caug-cc-pVDZ(cm+)	0.94872	24.188	1.0838	6.0529	1.0299	15.164
$CF_4(T_2)$	caug-cc-pVTZ(cm+)	1.0060	16.176	0.9877	10.535	1.0247	15.479
	caug-cc-pVDZ(cm+)	1.0010	14.521	1.0916	11.890	1.1124	18.417
$CF_4(A_1)$	caug-cc-pVTZ(cm+)	0.9807	19.842	1.0154	15.300	1.0120	15.265

TABLE VII. Optimal values of θ for all single point energy calculations. θ is reported in polar form with the phase in degrees.

R(Å)	$\|s\|$	phase[s]
1.08	0.9277	11.639
1.10	1.0998	15.963
1.12	0.9498	11.797
1.14	0.9849	10.117
1.16	1.0154	8.9519
1.18	0.9346	11.334
1.20	0.9495	10.702
1.22	0.9204	11.089
1.24	0.9598	10.566
1.26	0.9655	10.324
1.28	0.9738	9.4073
1.30	1.0000	9.9328
1.32	0.9808	10.255
1.34	0.9981	9.9255
1.36	1.0000	4.0001
1.38	0.9822	9.2917
1.40	1.0051	9.1503
1.42	0.9710	8.7806
1.44	1.0036	9.2459
1.46	0.9799	8.9373
1.48	0.9950	8.8133
1.50	0.9972	8.9010
1.52	0.9981	8.9202
1.54	1.0010	8.9371
1.56	1.0011	8.9626
1.58	1.0009	8.9886
1.60	1.0016	9.0031
1.62	1.0016	9.0394
1.64	0.9983	9.0643
1.66	0.9958	9.0609
1.68	0.9946	9.1075
1.70	0.9907	8.9882

TABLE VIII. Optimal values of θ for all points on the carbon monoxide PES. θ is reported in polar form with the phase in degrees.